DeLong and G. P. Meisner, *Solid State Commun.* **53**, 119 (1985).
12. D. T. Morelli and G. P. Meisner, *J. Appl. Phys.* **77**, 3777 (1995).
13. Z. Fisk, P. C. Canfield, J. D. Thompson, M. F. Hundley, *J. Alloys Compounds* **181**, 369 (1993); B. C. Sales *et al.*, *Phys. Rev. B* **50**, 8207 (1994).
14. T. Caillat, A. Borshchevsky, J.-P. Fleurial, in *Proceedings of the XIth International Conference on Thermoelectrics*, K. R. Rao, Ed. (Univ. of Texas at Arlington Press, Arlington, 1993), pp. 98–102.
15. G. A. Slack and V. G. Tsoukala, *J. Appl. Phys.* **76**, 1665 (1994); D. Mandrus *et al.*, *Phys. Rev. B* **52**, 4926 (1995); J.-P. Fleurial, T. Caillat, A. Borshchevsky, in *Thirteenth International Conference on Thermoelectrics*, B. Mathiprakasam and P. Heenan, Eds. (AIP Conference Proceedings No. 316, American Institute of Physics, New York, 1995), pp. 40–44.
16. D. T. Morelli *et al.*, *Phys. Rev. B* **51**, 9622 (1995).
17. J. W. Sharp, E. C. Jones, R. K. Williams, P. M. Martin, B. C. Sales, *J. Appl. Phys.* **78**, 1013 (1995).
18. F. Hulliger, *Helv. Phys. Acta* **34**, 782 (1961); D. Dudkin and N. K. Abrikosov, *Sov. Phys. Solid State* **1**, 126 (1959).
19. D. Jung, M.-H. Whangbo, S. Alvarez, *Inorg. Chem.* **29**, 2252 (1990); D. J. Singh and W. E. Pickett, *Phys. Rev. B* **50**, 11235 (1994).
20. B. C. Sales, unpublished data.
21. R. K. Williams, R. K. Nanstad, R. S. Graves, R. G. Berggren, *J. Nucl. Mater.* **115**, 211 (1983).
22. Flashline-5000 (Anter Corporation, Pittsburgh, PA). The data from this instrument were calibrated with a National Institute of Standards and Technology stainless steel standard.
23. Sponsored in part by a Cooperative Research and Development Agreement with Marlow Industries, contract CRADAX94-0324, and in part by the Division of Materials Sciences, U.S. Department of Energy contract DE-AC05-96OR22464. We thank H. B. Lyon, J. W. Sharp, G. A. Slack, J.-P. Fleurial, T. Callait, J. O. Sofo, and G. D. Mahan for illuminating discussions; R. B. Dinwiddie and H. Wang for thermal diffusivity measurements on several samples from 300 to 800 K; and P. M. Martin for helping with the precise thermal conductivity measurements near room temperature.

23 January 1996; accepted 19 March 1996

Crystal Structure of the Dual Specificity Protein Phosphatase VHR

Jirundon Yuvaniyama, John M. Denu, Jack E. Dixon, Mark A. Saper*

Dual specificity protein phosphatases (DSPs) regulate mitogenic signal transduction and control the cell cycle. Here, the crystal structure of a human DSP, vaccinia H1-related phosphatase (or VHR), was determined at 2.1 angstrom resolution. A shallow active site pocket in VHR allows for the hydrolysis of phosphorylated serine, threonine, or tyrosine protein residues, whereas the deeper active site of protein tyrosine phosphatases (PTPs) restricts substrate specificity to only phosphotyrosine. Positively charged crevices near the active site may explain the enzyme's preference for substrates with two phosphorylated residues. The VHR structure defines a conserved structural scaffold for both DSPs and PTPs. A "recognition region," connecting helix α1 to strand β1, may determine differences in substrate specificity between VHR, the PTPs, and other DSPs.

The protein encoded by the H1 open reading frame in vaccinia virus was identified as the first dual specificity protein phosphatase (DSP), capable of hydrolyzing phosphate monoesters from peptides containing either phosphotyrosine or phosphoserine (*1*). The $p80^{CDC25}$ protein, which is necessary for regulating the M phase transition during the cell cycle (*2*), showed limited sequence identity to the vaccinia phosphatase (*3*). The $p80^{CDC25}$ protein has intrinsic phosphatase activity and activates the $p34^{CDC2}$-cyclin protein kinase complex by dephosphorylating adjacent residues Thr^{14} and Tyr^{15} (*4*).

More than 20 mammalian DSPs have now been identified. Two of them, MKP-1 (*5*) and PAC-1 (*6*), regulate mitogenic signal transduction by dephosphorylating both Thr^{183} and Tyr^{185} residues on the mitogen-activated protein (MAP) kinase (*5*, *7*). A vaccinia H1-related phosphatase (VHR) was identified in humans and shown to be a DSP (*8*). VHR can hydrolyze phosphotyrosine and phosphothreonine residues on peptides derived from MAP kinase (*9*) and can activate maturation promotion factor when injected into *Xenopus* oocytes (*10*). Mutagenesis of Cys^{124} abolished all phosphatase activity, which suggests that the enzyme contains a single active site (*8*). Recombinant VHR is the archetypal phosphatase used in studies designed to elucidate the catalytic mechanism of the DSPs (*11–14*).

To understand the structural determinants of specificity and function of this enzyme family, we solved the three-dimensional structure of VHR to 2.1 Å resolution by x-ray crystallography (*15*) (Table 1). A typical example of the "omit" electron density map is presented in Fig. 1. VHR consists of a single α+β-type domain of dimensions 50 Å by 40 Å by 32 Å. The loop between the β8 strand and α5 helix (residues 123 to 131) (Fig. 1, also Fig. 4A) contains the consensus active-site sequence His-Cys-X-X-Gly-X-X-Arg-(Ser or Thr) (*16*) with the catalytic Cys^{124} thiol at its center (X is any amino acid). In the crystal structure, the competitive inhibitor sulfate is bound at the active site (Fig. 1). The oxygen atoms of sulfate form hydrogen bonds to the main chain amides of the active site loop and to the Arg^{130} side chain, mimicking the corresponding interactions between the phosphate oxygens on a phosphoprotein substrate.

To explore the structural basis for how VHR can bind and dephosphorylate either phosphotyrosine, phosphothreonine, or phosphoserine residues, we compared the active sites of VHR and those of two protein tyrosine phosphatases (PTPs), *Yersinia* PTP (*17*, *18*) and human PTP1B (*19*, *20*). The specificity of PTP1B for phosphotyrosine, and not for phosphothreonine, is determined primarily by the depth of the active site cleft (*20*). Although the active site loop, termed the P-loop in the *Yersinia* enzyme, is structurally conserved among both PTPs and DSPs, cross sections of the VHR and the *Yersinia* PTP active sites revealed a disparity in the depth of the active site clefts (Fig. 2). The active site pocket of VHR is at most 6 Å deep and is surrounded by side chains mainly from the P-loop itself. In contrast, the depth of the *Yersinia* PTP and PTP1B (*20*) active site cleft is about 9

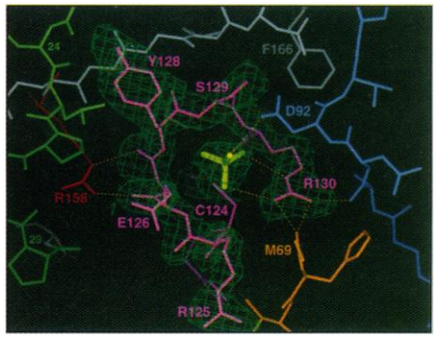

Fig. 1. VHR catalytic site with the P-loop (magenta) containing the catalytic Cys^{124} and a bound sulfate anion (yellow) (*33*). Hydrogen bonds are shown in dashed lines. The main chain amides of the P-loop make six additional hydrogen bonds (not shown) with the three sulfate oxygens. Contoured at 2.3σ (dark green) is a 2.1 Å resolution "omit" map in which the P-loop atoms and sulfate were not included in the simulated-annealing refinement before map calculation. Portions of the structure are similarly colored in all figures: the general acid loop (residues 88 to 98) between β7 and α4 is blue, the α1-β1 or "recognition region" (residues 19 to 29) is green, and the "variable insert" between β3 and β7 (residues 62 to 82) is orange. Red shows Arg^{158}.

J. Yuvaniyama and M. A. Saper, Biophysics Research Division and Department of Biological Chemistry, University of Michigan, Ann Arbor, MI 48109–1055, USA.
J. M. Denu and J. E. Dixon, Department of Biological Chemistry, University of Michigan, Ann Arbor, MI 48109–0606, USA.

*To whom correspondence should be addressed. E-mail: saper@umich.edu

Å and includes an upper ridge formed by residues 229 to 232. Short peptides containing phosphotyrosine or phosphothreonine residues were modeled into the substrate clefts (*21*). Either phosphotyrosine or phosphothreonine can bind to the shallow active site of VHR. In contrast, only the longer Tyr phosphoester can reach the nucleophilic Cys located at the base of the *Yersinia* PTP active site. Thus, the phosphoamino acid specificity of DSPs appears to be governed in part by the shallow active site pocket.

A water molecule can be found in the active sites of *Yersinia* PTP (*18*) (Fig. 2B) and PTP1B (*20*). It is ligated by the substrate phosphate and a glutamine conserved in PTPs (Gln^{450} in *Yersinia* PTP). A similarly positioned water molecule or cavity is absent in the VHR structure (Fig. 2A) and may be absent in other DSPs. Residues Ser^{129} and Asp^{92} occupy the position of the water molecule in the VHR structure and are conserved in other DSP sequences. Also, DSPs have a hydrophobic residue (Phe^{166} in VHR) (Figs. 1 and 2) in a position corresponding to that of the *Yersinia* PTP Gln^{450}. Active site differences such as these suggest potential rationales for the design of inhibitors that would discriminate between PTPs and DSPs.

VHR has a preference toward substrates containing a second phosphorylated side chain located two residues NH_2-terminal of a phosphotyrosine residue (*9*). A secondary binding site may exist in VHR to recognize the other phosphorylated residue. Surface grooves connect the active site pocket to other positively charged pockets centered near Arg^{125}, Arg^{130}, and Arg^{158} (Fig. 3). It is unlikely that the Arg^{130} pocket ligates the second phosphorylated residue, as the hydrogen-bonding potential of Arg^{130} is completely fulfilled. In contrast, the Arg^{125} and Arg^{158} pockets are available for hydrogen bond interactions and are about 9 Å from the catalytic site. The Arg^{158} pocket is connected to the active site by a small groove between Glu^{126} and Tyr^{128} on the P-loop (Fig. 1) and is surrounded by residues 25 to 29 on the α1-β1 loop, Gln^{41} on the α2 helix, and Glu^{126}. Arg^{125} emanates from the P-loop (Fig. 1) and forms the side of a shallow depression on the surface of the enzyme (Fig. 3).

Although the DSPs have sequence similarity only to the PTP active-site consensus sequence, the structure of VHR reveals a general fold that occurs in the *Yersinia* PTP and PTP1B (Fig. 4A). All secondary structural elements in VHR, except α2′ and α3, have corresponding structural homologs in both PTPs. From the superposition (*22*) of the three structures, we constructed a structure-based sequence alignment (Fig. 4B). Although smaller than that of the PTPs, the VHR structure retains the same starting and ending secondary structure elements as the catalytic domain of the PTPs. This suggests that the VHR structure may define a minimal core structure for both DSPs and PTPs.

The α1-β1 loop in VHR (green, Fig. 4) is one-fourth the length of the equivalent region found in the *Yersinia* PTP and PTP1B. The crystal structure of PTP1B complexed with a phosphotyrosine peptide (*20*) revealed that this 41-residue region was directly involved in substrate binding: Arg^{47} and Asp^{48} made important hydrogen-bonding interactions to acidic residues and main chain atoms, respectively, of the polypeptide substrate, and Tyr^{46} and Val^{49} made van der Waals interactions with the aromatic ring of the phosphotyrosine substrate. The *Yersinia* PTP α1-β1 region has a different sequence from that of PTP1B, but a similar four-residue motif, Phe-Arg-Asp-Ile (residues 229 to 232), makes identical interactions with bound peptides (*23*). These residues, present in most PTPs, contribute to the overall depth of the active site cleft (Fig. 2B). In contrast, the corresponding residues are absent in the VHR structure, providing a shallow active site pocket that accounts for its dual specificity (Fig. 2A). Moreover, the shorter α1-β1 loop of VHR exposes the conserved Arg^{158} and opens a positively charged site, possibly for substrate binding. The corresponding Arg^{440} of *Yersinia* PTP (Arg^{257} in PTP1B) is buried by the α1-β1 loop, and no similar

Table 1. VHR data collection and phasing statistics (*15*). Crystal space group is $P2_1$, a = 61.15 Å, b = 60.04 Å, c = 52.02 Å, and β = 98.35°, with two molecules per asymmetric unit. A total of 8938 reflections were phased (10–2.8 Å) with a mean figure of merit of 0.58.

Derivative	Resolution (Å)	Observed/ unique reflections	Completeness (%)	R_{sym}*	R_{iso}†	MIR phasing power‡
Native	2.1	41,078/18,952	86	5.5	—	—
3 mM Na_3WO_4	2.1	50,397/20,632	94	5.8	15.2	1.8
10 mM $(CH_3)_3PbOAc$	2.5	31,922/12,209	92	7.0	11.9	1.9
5 mM $(CH_3)_3PbCl$	2.5	38,014/12,659	96	7.3	16.8	2.1

*$R_{sym} = (\Sigma|I_i - \langle I\rangle|/\Sigma I_i) \times 100$, where I_i is the intensity of individual observations and $\langle I\rangle$ is the mean intensity. †$R_{iso} = (\Sigma||F_{PH}| - |F_P||/\Sigma|F_{PH}|) \times 100$, where F_P and F_{PH} are native and derivative structure factors, respectively. ‡MIR phasing power, rms F_H/E, where E is the residual lack of closure error and F_H is the heavy atom structure factor.

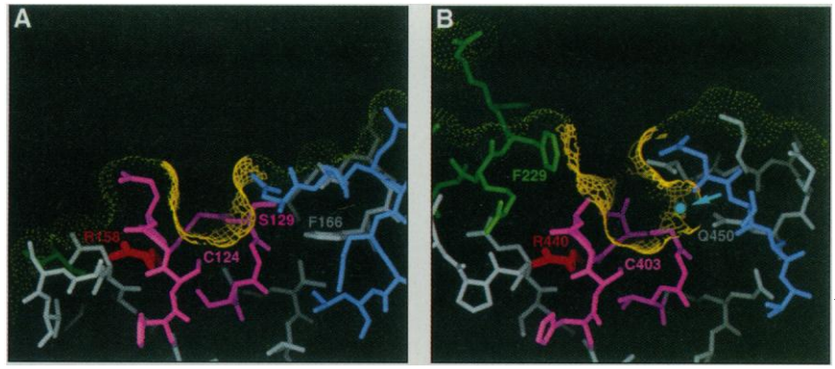

Fig. 2. Dual specificity of VHR conferred by the shallow active site pocket. Sliced views of the active sites of VHR (**A**) and the *Yersinia* PTP-sulfate complex [Protein Data Bank (PDB) entry 1YTS] (**B**). Yellow dots and mesh represent the solvent contact surfaces (*34*) that reveal the different depths of the two active-site pockets. Green residues in (B) are from the recognition region (Fig. 4). The cyan arrow points to a structural water molecule that is involved in ligand binding to the PTP but is absent in the VHR structure.

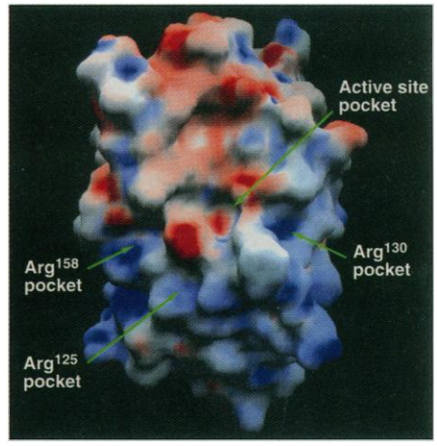

Fig. 3. The binding surface of VHR. The VHR molecular contact surface shows the electrostatic potential colored from −15 *kT* (red) to 15 *kT* (blue) (where *k* is the Boltzmann constant and *T* is the absolute temperature). There are three positively charged pockets near the active site of VHR, designated Arg^{125}, Arg^{130}, and Arg^{158}. Figure was drawn with GRASP (*35*).

charged pocket is observed. We propose the term "recognition region" for the chain connecting α1 and β1 in PTP structures and VHR because of its variability and effect on substrate recognition.

Another major structural difference between VHR and the PTPs is the β3 to β7 region (orange, Fig. 4). In VHR, β3 is followed by a meandering loop and a 3_{10} helix (α3) before entering β7 (Fig. 4A). This crossover is nearly four times longer in the PTPs and contains an antiparallel β sheet. The initial residues of the β3 to β7 region, though different in primary and tertiary structure, are essential for the integrity of both the DSP and PTP active site. In PTPs, an invariant and catalytically important Glu (Glu[115] in PTP1B) forms a bidentate salt bridge with the active site Arg (Arg[221] in PTP1B). In VHR, Arg[130] is anchored by the main chain carbonyl of Met[69] (Fig. 1). Other portions of the PTP chain between β3 to β7 are variable in sequence and have no known function. Therefore, we propose the term "variable insert" for the β3 to β7 region of DSP and PTP structures.

There are only 10 identical amino acids between VHR and the PTPs in a structure-based sequence alignment (Fig. 4B). Most of these conserved residues are critical in catalysis and are located near the active site, which suggests that a common catalytic mechanism may be used by both the DSPs and the PTPs. The catalytic Cys[124] of VHR functions as the active site nucleophile that attacks the phosphorus atom of a substrate to form a phosphoenzyme intermediate (*11*). The conserved hydroxyl of Ser[131] is essential for efficient hydrolysis of the phosphoenzyme intermediate (*13*). Asp[92] acts as a general acid by protonating the leaving phenolic oxygen in phosphotyrosine-containing substrates (*12*). This same aspartic acid residue functions as a general base during the hydrolysis of the phosphoenzyme intermediate by activating a water molecule (*14*). Although the analogous aspartic acid of PTP1B or *Yersinia* PTP has a similar catalytic function, Asp[92] of VHR is located on a different side of the active site and may protonate the phosphate ester oxygen from a different angle than that observed in the PTPs. Consequently, the bound sulfate is not shielded from bulk solvent as in the PTPs (*18*) but appears free to enter and leave the shallow pocket of VHR.

Other DSPs are likely built on a VHR core structure. Sequence alignment of DSPs CL100 (human homolog of MKP-1) (*24*) and PAC-1 show approximately 30% sequence identity with VHR between β1 and the COOH-terminus (*25*). As with the PTPs, the major differences between VHR and the catalytic domains of other DSPs occur within the "recognition region" between α1 and β1 and within the "variable insert" located between β3 and β7. Residues 1 to 122 of CL100, including the segments similar to those of the p80[CDC25] phosphatase (*24*), are unaccounted for in our alignment, suggesting that they are not part of the DSP core structure and may form a distinct structural domain. Amino acids 1 to 122 constitute exon 1 of the gene encoding CL100 (*24*), which suggests that CL100 may have resulted from the fusion of exon 1 with a preexisting phosphatase gene resembling VHR.

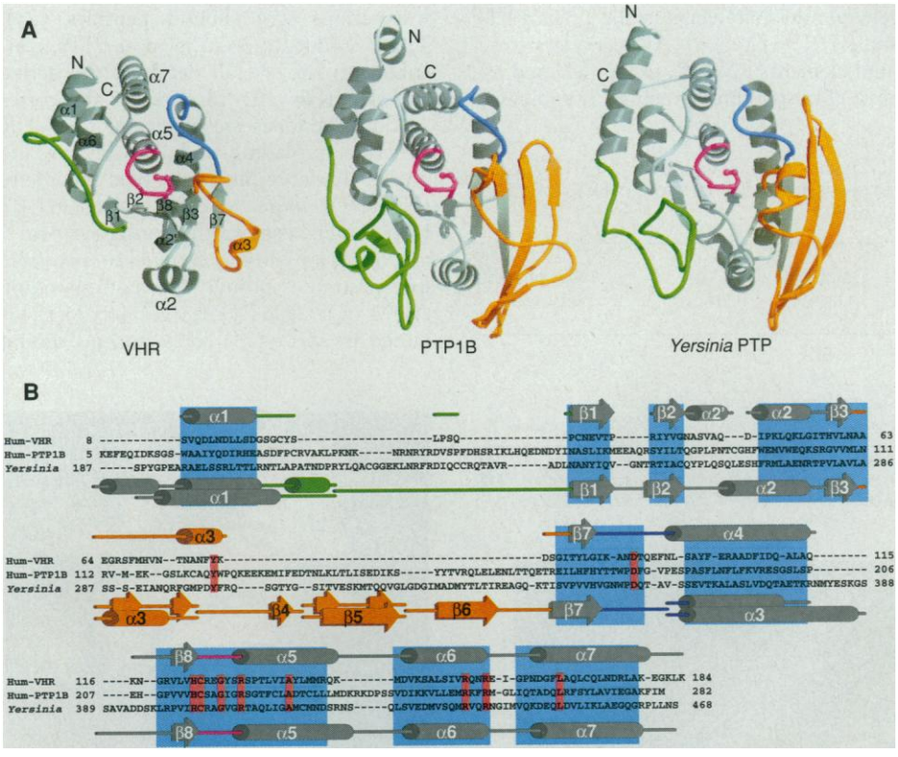

Fig. 4. Structural comparison between the DSP VHR and the PTPs. (**A**) Schematic diagrams showing the VHR, human PTP1B (*19*) (PDB entry 2HNQ), and the *Yersinia* PTP Yop51 (*18*) (PDB entry 1YTS) structures drawn in a common orientation and scale. Superposition (*22*) of the Cα backbone of VHR to PTP1B and the *Yersinia* PTP yielded a rmsd of 1.84 Å for 121 Cα's and 1.68 Å for 109 Cα's, respectively. See Fig. 1 for explanation of the colors. The two major differences are the "recognition region" in green and the "variable insert" in orange. (**B**) Structure-based sequence alignment (*33*). Portions of the sequences judged structurally equivalent by the Lsq_improve algorithm in O (*22*) are shaded blue. The 10 residues conserved in all three structures are pink. Immediately above the sequence alignment are the secondary structure designations for VHR (arrows, strands; cylinders, helices). Below the sequence alignment are the designations for the two PTPs. Where they differ, *Yersinia* PTP is in front and PTP1B is in back. The naming of the secondary structure elements follows that used for the *Yersinia* PTP structure (*17*). The α1-β1 loop in VHR is shown in green; N and C, NH_2- and COOH-terminus, respectively.

REFERENCES AND NOTES

1. K. Guan, S. S. Broyles, J. E. Dixon, *Nature* **350**, 359 (1991).
2. S. Moreno, P. Nurse, P. Russell, *ibid.* **344**, 549 (1990).
3. S. Moreno and P. Nurse, *ibid.* **351**, 194 (1991).
4. J. Gautier, M. J. Solomon, R. N. Booher, J. F. Bazan, M. W. Kirschner, *Cell* **67**, 197 (1991); W. G. Dunphy and A. Kumagai, *ibid.*, p. 189; U. Strausfeld *et al.*, *Nature* **351**, 242 (1991).
5. H. Sun, C. H. Charles, L. F. Lau, N. K. Tonks, *Cell* **75**, 487 (1993).
6. P. J. Rohan *et al.*, *Science* **259**, 1763 (1993).
7. Y. Ward *et al.*, *Nature* **367**, 651 (1994).
8. T. Ishibashi, D. P. Bottaro, A. Chan, T. Miki, S. A. Aaronson, *Proc. Natl. Acad. Sci. U.S.A.* **89**, 12170 (1992).
9. J. M. Denu *et al.*, *J. Biol. Chem.* **270**, 3796 (1995).
10. P. Aroca, D. P. Bottaro, T. Ishibashi, S. A. Aaronson, E. Santos, *ibid.*, p. 14229.
11. G. Zhou, J. M. Denu, L. Wu, J. E. Dixon, *ibid.* **269**, 28084 (1994).
12. J. M. Denu, G. Zhou, Y. Guo, J. E. Dixon, *Biochemistry* **34**, 3396 (1995).
13. J. M. Denu and J. E. Dixon, *Proc. Natl. Acad. Sci. U.S.A.* **92**, 5910 (1995).
14. J. M. Denu, D. L. Lohse, J. Vijayalakshmi, M. A. Saper, J. E. Dixon, *ibid.* **93**, 2493 (1996).
15. The expression, purification, and crystallization of human VHR have been described (*9*). Crystals were grown in hanging drops of 20 μl containing VHR (5 mg/ml), 10 to 15% polyethylene glycol 4000, 22 mM Li_2SO_4, 0.1% β-mercaptoethanol, and 50 mM Hepes (pH 7.0) and equilibrated at 22°C against twice the concentration of the same precipitant solution. The two trimethyllead derivatives each had the same two binding sites (near Cys[30] Sγ), but with relatively different occupancies. Diffraction images were collected at 22°C on an SDMS multiwire area detector mounted on a Rigaku RU200 generator (50 kV, 100 mA). Reflections were integrated with MADNES (*26*) and scaled with XSCALE (*27*). Heavy atom refinement and multiple isomorphous replacement (MIR) phasing were done with PHASES (*28*). The noncrystallographic symmetry (NCS) operator was refined and the MIR map iteratively averaged

with RAVE (*29*). Phases calculated from an initial model traced with O (*22*) were combined with the MIR phase probabilities (*30*) to further improve the electron density maps. The model was refined with XPLOR (*31*). NCS restraints were applied at early stages but then removed. The final *R* factor to 2.1 Å was 17.6% (16,879 reflections) and the R_{free} (*32*) was 25.4% (1867 reflections) for 2929 atoms (residues 8 to 185 in two VHR molecules, one sulfate, one Hepes, and 141 ordered water molecules). The root mean square deviation (rmsd) from ideal bonds and angles was 0.016 Å and 1.7 Å, respectively. The rmsd between the two NCS-related molecules was 1.26 Å for all atoms and 0.82 Å for main chain atoms. The VHR coordinates are available from the Brookhaven Protein Data Bank as entry 1VHR.

16. R. L. Stone and J. E. Dixon, *J. Biol. Chem.* **269**, 31323 (1994).
17. J. A. Stuckey *et al.*, *Nature* **370**, 571 (1994).
18. H. L. Schubert, E. B. Fauman, J. A. Stuckey, J. E. Dixon, M. A. Saper, *Protein Sci.* **4**, 1904 (1995).
19. D. Barford, A. J. Flint, N. K. Tonks, *Science* **263**, 1397 (1994).
20. Z. Jia, D. Barford, A. J. Flint, N. K. Tonks, *ibid.* **268**, 1754 (1995).
21. J. Yuvaniyama *et al.*, data not shown. The peptides modeled were Ala-phosphothreonine-Ala and Ala-phosphotyrosine-Ala.
22. T. A. Jones, J. Y. Zou, S. W. Cowan, M. Kjeldgaard, *Acta Crystallogr.* **A47**, 110 (1991).
23. J. A. Stuckey and M. A. Saper, unpublished data.
24. S. P. Kwak, D. J. Hakes, K. J. Martell, J. E. Dixon, *J. Biol. Chem.* **269**, 3596 (1994).
25. We used the secondary structure of VHR and the secondary structure predicted for CL100 and PAC-1 [B. Rost, C. Sander, R. Schneider, *Comput. Appl. Biosci.* **10**, 53 (1994)] together with the CLUSTALV program [D. G. Higgins, A. J. Bleasby, R. Fuchs, *ibid.* **8**, 189 (1992)] to construct a sequence alignment of the three DSPs. To locate the start of the catalytic domain in CL100, corresponding to the α1 helix in VHR, we scanned upstream terminus of the β1 strand for predicted helices in the CL100 sequence that had the best primary sequence alignment with VHR. The catalytic domains of CL100 and PAC-1 were predicted from the alignment to begin at residues 123 and 130, respectively.
26. A. Messerschmidt and J. W. Pflugrath, *J. Appl. Crystallogr.* **20**, 306 (1987).
27. W. Kabsch, *ibid.* **21**, 916 (1988).
28. W. Furey and S. Swaminathan, *Am. Cryst. Assoc. Meeting Abst.* **18**, 73 (1990).
29. G. J. Kleywegt and T. A. Jones, in *From First Map to Final Model*, S. Bailey, R. Hubbard, D. Waller, Eds. (Engineering and Physical Sciences Research Council, Daresbury, UK, 1994), pp. 59–66.
30. R. J. Read, *Acta Crystallogr.* **A46**, 140 (1990).
31. A. T. Brünger, J. Kuriyan, M. Karplus, *Science* **235**, 458 (1987).
32. A. T. Brünger, *Nature* **355**, 472 (1992).
33. Abbreviations for the amino acid residues are as follows: A, Ala; C, Cys; D, Asp; E, Glu; F, Phe; G, Gly; H, His; I, Ile; K, Lys; L, Leu; M, Met; N, Asn; P, Pro; Q, Gln; R, Arg; S, Ser; T, Thr; V, Val; W, Trp; and Y, Tyr.
34. M. L. Connolly, *J. Appl. Crystallogr.* **16**, 548 (1983).
35. A. Nicholls, K. A. Sharp, B. Honig, *Proteins* **11**, 281 (1991).

36. We thank M. Wishart for help with the CL100 and PAC-1 alignments and C. Yuvaniyama for technical support. Supported by the NIH (grant AI34095 to M.A.S. and grants DK18024 and DK18849 to J.E.D.), a National Research Service award to J.M.D. (GM17789), the University of Michigan Multipurpose Arthritis Center (NIH grant P60-AR20557), and Mitotix Inc. J.Y. is a scholar of the Thai Development and Promotion of Science and Technology Talents Project. M.A.S. is a Pew Scholar in the Biomedical Sciences.

28 November 1995; accepted 8 March 1996

Dimerization of TFIID When Not Bound to DNA

Andrew K. P. Taggart and B. Franklin Pugh*

For unknown reasons, the eukaryotic transcription factor TFIID inefficiently recognizes promoters. Human TFIID was found to form highly specific homodimers that must dissociate before DNA binding. TFIID dimers formed through self-association of the TATA-binding polypeptide (TBP) subunit and could be immunoprecipitated with antibodies to $TAF_{II}250$, the core subunit of TFIID. Chemical cross-linking experiments in HeLa cells revealed the presence of TBP dimers in vivo. These findings suggest that dimerization through TBP is the physiological state of TFIID when not bound to DNA. Thus, the inefficiency of TFIID binding to a promoter may be partly attributable to the competitive effect of dimerization.

Transcription of eukaryotic genes requires the formation of a preinitiation complex containing one of three nuclear RNA polymerases and additional basal factors (*1*). Sequence-specific transcriptional activators function, in part, through direct interactions with basal factors, including polymerase-specific TBP-TAF complexes such as SL1, TFIID, and TFIIIB (*2*). In RNA polymerase II transcription of mRNA genes, the binding of TFIID to the promoter is rate-limiting in complex assembly (*3*). Activators might enhance the recruitment of TFIID to the promoter by targeting TAFs (TBP-associated factors) and TFIIA (*3*); however, the exact mechanism by which TFIID is recruited is not known.

The conserved core DNA-binding domain of TBP homodimerizes at low nanomolar concentrations (*4*). Consequently, TBP dimers must dissociate into monomers before they can bind DNA. These findings are consistent with the reported dimeric crystal structure of TBP dimers (*5*). Because TBP is generally complexed with TAFs, the physiological significance of dimerization is dependent on whether TBP-TAF complexes also dimerize.

To test whether TFIID dimerizes, we subjected a partially purified HeLa TFIID fraction (P.7), which contained approximately 20 to 30 nM TBP, to chemical crosslinking with the use of bis(maleimido)hexane (BMH). In the absence of BMH, the TBP present in the P.7 fraction migrated on an SDS-polyacrylamide gel, with a molecular mass of 44 kD (Fig. 1A). In the presence of BMH, a 90-kD species appeared in the P.7 fraction with a mobility indistinguishable from that of cross-linked recombinant TBP dimers. No other major crosslinker-dependent TBP-containing species was detected, even though the TFIID was <0.1% pure. The predominance of the 90-kD species, among a >1000-fold molar excess of nonspecific nuclear proteins, re-

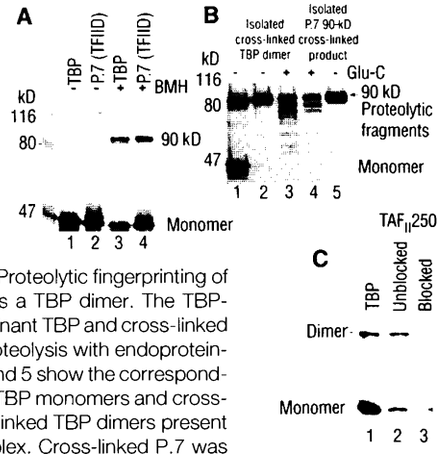

Fig. 1. TBP-TBP cross-linking of TFIID in a crude fraction. (**A**) Crosslinking of the TFIID fraction results in a single TBP-containing 90-kD product. P.7 (TFIID) or purified recombinant TBP were incubated briefly in the absence (−, lanes 1 and 2) or presence (+, lanes 3 and 4) of BMH (*10*). P.7 (TFIID) was generated by passing HeLa nuclear extracts over phosphocellulose and taking a step elution of 0.5 to 0.7 M KCl. Reactions were analyzed by SDS-PAGE and protein immunoblotting with affinity-purified anti-TBP. The purity of the TBP was 99%, and that of the TFIID was <0.1%. (**B**) Proteolytic fingerprinting of the 90-kD band from cross-linked P.7 identifies it as a TBP dimer. The TBP-containing 90-kD products from cross-linked recombinant TBP and cross-linked P.7 (TFIID) were isolated and subjected to limited proteolysis with endoproteinase Glu-C (lanes 3 and 4, respectively) (*11*). Lanes 2 and 5 show the corresponding reaction performed in the absence of proteinase. TBP monomers and cross-linked dimer markers are shown in lane 1. (**C**) Cross-linked TBP dimers present in the P.7 (TFIID) fraction are part of the TFIID complex. Cross-linked P.7 was subjected to immunoprecipitation with anti-$TAF_{II}250$ in the absence (lane 2, unblocked) or presence (lane 3, blocked) of neutralizing $TAF_{II}250$ antigen (*12*). The immunoprecipitates were subjected to protein immunoblot analysis with anti-TBP. A TBP dimer marker is shown in lane 1.

Center for Gene Regulation, Department of Biochemistry and Molecular Biology, Pennsylvania State University, University Park, PA 16802, USA.

*To whom correspondence should be addressed. E-mail: bfp2@psuvm.psu.edu